Volume 1 | Number 1 | Jan 2013 | Pages 1–100

ChemComm

Chemical Communications
www.rsc.org/chemcomm

ROYAL SOCIETY
OF CHEMISTRY

www.rsc.org/chemcomm

ChemComm

COMMUNICATION

Nitrogen-doped bamboo-like carbon nanotubes: promising anode materials for sodium-ion batteries

Dongdong Li,[ab‡] Lei Zhang,[b‡] Hongbin Chen,[a] Liang-xin Ding,[*a] Suqing Wang[a] and Haihui Wang[*ab]

Nitrogen-doped bamboo-like carbon nanotubes (N-BCNTs) were synthesised using a facile one-step pyrolysis process. Due to their unique one-dimensional hollow structure and intrinsic high nitrogen content, N-BCNTs exhibit high capacity, superior rate capability, and excellent cycle stability and are, thus, promising anode materials for sodium-ion batteries.

Sodium-ion batteries (SIBs), which are "close relatives" of lithium-ion batteries (LIBs), have attracted increasing attention as a result of growing concerns regarding limited lithium reserves.[1-4] However, practical SIBs applications remain out of reach due to the lack of appropriate electrode materials. Carbon-based materials have been regarded as promising anode materials for SIBs due to carbon's high specific capacity and abundant resources. However, taking advantage of SIBs' exceptional sodium ion storage capability is difficult because of the sodium ion's low solid-state diffusion coefficient in carbon materials. Shortening the diffusion lengths of sodium ions in the solid phase is an effective means of facilitating sodium ion diffusion. Thus, nanostructured carbon-based materials have been investigated with the aim of improving their electrochemical applications as anode materials for SIBs. Nanostructures not only facilitates Na^+ transport by shortening diffusion distances but also increases the contact areas of electrode/electrolyte interfaces,[5-13] for instance, via nanospheres,[6] hollow spheres,[7, 8] nanofibers,[9, 10] nanosheets,[11] *etc*.[5, 7, 8] Another approach is doping heteroatoms, such as nitrogen, into carbon, such that the disorder of the carbon is increased, which may facilitate sodium-ion transport in the carbon solid phase.[14-16] Likewise, nitrogen doping could enhance the electrical conductivity of carbon materials.[17] However, when used alone, each design

strategy causes only limited improvements in the sodium storage performance of carbon-based materials. The synergetic effects of structure and composition have been considered as an effective means to further enhance sodium storage performance.[18-20] For example, Cao *et al.* found that a high reversible capacity of 149 mA h g^{-1} could be achieved, even at a high current density of 500 mA g^{-1}, by nitrogen-doped hollow carbon nanofibers.[18] Despite the progress achieved to date, research regarding the synergetic effects of nanostructure and composition is still in the early stage.

Herein, we report the synthesis of nitrogen-doped bamboo-like carbon nanotubes (N-BCNTs) via a one-step pyrolysis process, which simultaneously integrates a unique one-dimensional bamboo-like structure with intrinsically high nitrogen content. When tested as anode materials for SIBs, these N-BCNTs manifest high specific capacity (270 mA h g^{-1} at 50 mA g^{-1}) and excellent cycling stability.

N-BCNTs were synthesised via one-step pyrolysis process using a dicyandiamide (DCD) and $CoCl_2$ mixture (fabrication details are described in the Experimental details contained in ESI†.),[21-24] followed by acid etching. Fig. S1a (ESI†) displays the scanning electron microscopy (SEM) image of the pyrolysis product (Co@N-BCNTs@Co). It is obvious that the pyrolysis product has a one-dimensional (1D) structure, which was further shown to be a bamboo-like hollow structure by transmission electron microscope (TEM) analysis (Fig. S1b, ESI†). In addition, there is a nanoparticle at the tip of each bamboo-like tube, which is shown by XRD to be Co (Fig. S2 and Fig. S3, ESI†). It appears that this Co first appears in the initial stage of the pyrolysis and then catalyses the formation of a bamboo-like carbon nanotube.[25-27] After removing the Co nanoparticles via etching using an HCl aqueous solution, the products of N-BCNTs appear to be uniform, one-dimensional structures that are 200-300 nm in diameter and several micrometres in length (Fig. 1a). Moreover, no obvious Co nanoparticles can be seen inside the nanotube (Fig. 1b). Fig. 1c shows a magnified TEM image of the N-BCNTs, from which the wall thickness is determined to be approximately 10 nm. Fig. 1d shows a typical HRTEM image of the wall of N-BCNTs, in which the graphene layers are parallel to the axis direction of the N-BCNTs. The spacing between the graphene layers is approximately 0.36 nm, which is

a. School of Chemistry & Chemical Engineering, South China University of Technology, Guangzhou, 510640, PR China. E-mail: lxding@scut.edu.cn; hhwang@scut.edu.cn.
b. School of Chemical Engineering, University of Adelaide, Adelaide, SA 5005, Australia.
‡ D. Li and L. Zhang contributed equally to this work.
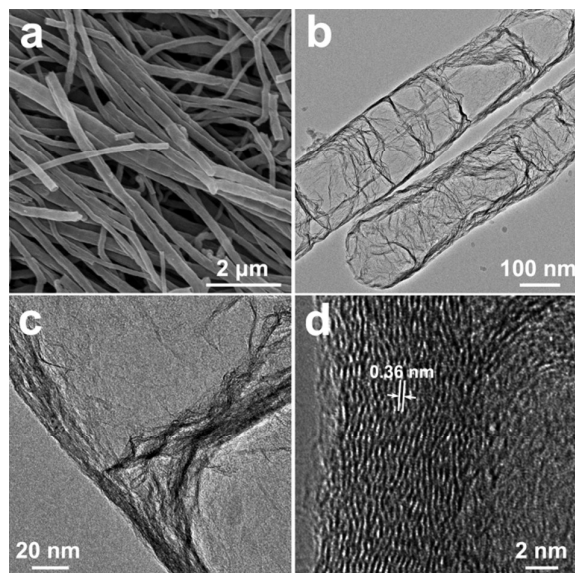
COMMUNICATION

Fig. 1 (a) SEM image of N-BCNTs; (b, c) TEM images of N-BCNTs; (d) HRTEM image of the wall of N-BCNTs.

larger than that of graphite (0.335 nm). HRTEM also found some small Co nanoparticles in the wall of the N-BCNTs. Fig. S4 shows the typical HRTEM image and a considerably lattice fringe with spacing of 0.21 nm is very consistent with the value of the (111) plane of Co. This result confirms the existence of Co species in N-BCNTs. Thermogravimetric analysis (TGA) was carried out to further identify the weight ratio of Co in N-BCNTs. As shown in the Fig. S5, the final weight ratio is 17.8 %. Furthermore, the Co would be converted to CoO at 900 ^{o}C. Thus, the weight ratio of the Co is calculated to be 14.0 %. By virtue of the bamboo-like structure and the ultrathin wall, the Brunauer-Emmett-Teller (BET) surface area of these N-BCNTs is calculated to be 122.6 m^2 g^{-1} (the N$_2$ sorption isotherm is given in Fig. S6a, ESI†). Furthermore, the analysis of pore size distribution (Fig. S6b, ESI†) reveals that the majority pore size is about 3.8 nm.
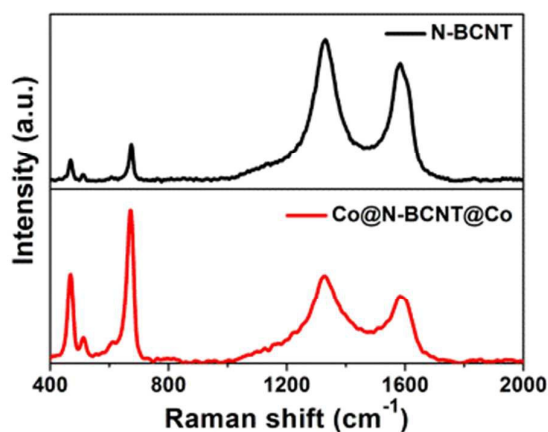

Fig. 2 Raman spectra of Co@N-BCNTs@Co and N-BCNT.

Fig. 2 shows the Raman spectra of Co@N-BCNTs@Co and N-BCNT. It is obvious that the DCD peaks (Fig. S7, ESI†) disappear after pyrolysis and that four new peaks appear at 1584, 1325, 672 and 469 cm^{-1} of Co@N-BCNTs@Co (Fig. 2). The peaks at 1325 and 1584 cm^{-1} correspond to the sp^3 graphitic configuration (D-band) and the sp^2 graphitic configuration (G-band), respectively, indicating that the DCD have been successfully carbonised.[19, 28] The peaks at 672 and 469 cm^{-1} are due to the presence of Co. The Raman spectrum of the final product, also presented in Fig. 2, clearly demonstrates a dramatic change in the peak intensities compared with that observed for Co@N-BCNT@Co. This change is due to the removal of Co from the N-BCNTs. The intensity ratio of the D-band over the G-band is 1.2, which agrees well with XRD (Fig. S3, ESI†) and HRTEM results for the amorphous structure.
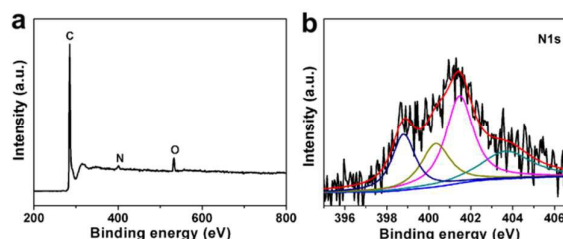

Fig. 3 XPS spectra of N-BCNTs: survey spectrum (a) and N1s spectrum (b).

To examine elemental composition and bonding configurations, X-ray photoelectron spectroscopy (XPS) was performed on N-BCNTs. As depicted in Fig. 3a, the survey spectrum shows only C, N, and O on the surface of the product lacking Co, indicating that the Co on the surface has been completely removed. In addition, the nitrogen atomic content calculated from XPS is 2.5%. The high-resolution XPS N1s spectrum can be deconvoluted into four different signals with binding energies of 398.8, 400.3, 401.5, and 403.7 ev, which correspond to pyridinic nitrogen, pyrrolic nitrogen, graphitic nitrogen and N-O bonding, respectively (Fig. 2b).[29, 30] Furthermore, we proved that the nitrogen content can be adjusted by changing the pyrolysis time.[31] Elemental analysis was used to investigate the samples from different pyrolysis times. The results (Table S1) proved that the nitrogen/carbon ratio decreases with the prolonging of the pyrolysis time. In addition, the bamboo-like structure can be retained at different pyrolysis times (Fig. S8).

The sodium-ion storage performances of N-BCNTs were first investigated using cyclic voltammetry (CV) in the voltage range of 0.01–3.0 V versus Na/Na$^+$. As shown in Fig. 4a, in the first cathodic scan, there are three peaks at 1.3, 0.7 and 0 V, which could be attributed to the reaction between Sodium-ions and surface functional groups, the formation of a solid electrolyte interface (SEI) film, and the insertion of Sodium-ions into the N-BCNTs, respectively.[7, 10, 14, 16] In the following cathodic scans, the peak at 1.3 V disappeared due to the existence of an SEI film. Notably, the peak at 0.7 V exists until the 6th scan, indicating that a stable SEI film is formed after 5 cycles. For the anodic scans, no obvious peak is observed, indicating that the extraction of Sodium-ions from carbonaceous materials has no specific voltage range. From the 6th cycle onwards, the CV curves mostly overlap, indicating good reversibility of the electrochemical reactions. Electrochemical

performance was also evaluated using galvanostatic discharge-charge, as shown in Fig. 4b, the results of which agree well with the CV results. Fig. 4c shows the cycle performance of N-BCNTs at different current density. The reversible capacity of the N-BCNTs is as high as 270.6 mAh g^{-1} at the current density of 50 mA g^{-1}. Furthermore, the N-BCNTs exhibit excellent rate performance, with reversible capacities of 167, 138, 104, and 81 mAh g^{-1} at current densities of 0.1, 0.2, 0.5, and 1.0 A g^{-1}, respectively. After rate testing, the same cell was further evaluated in terms of its long cycle stability at a current density of 0.5 A g^{-1}, as shown in Fig. 4d. The capacity shows almost no change from the 60th cycle to the 160th cycle. In addition, the coulombic efficiency is maintained at 99% for all cycles, demonstrating the excellent cycle stability of N-BCNTs.
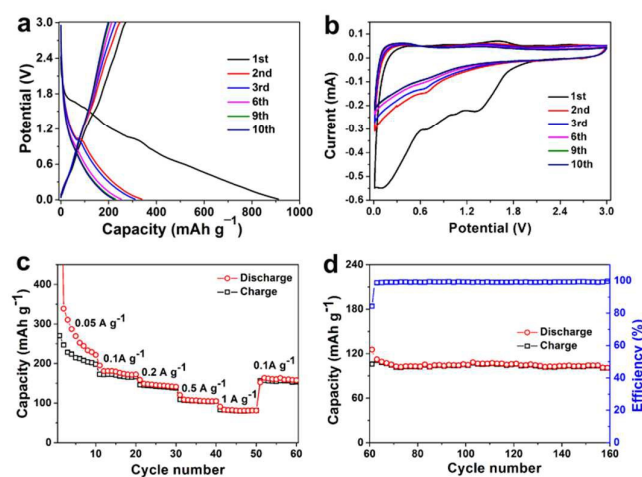

Fig. 4 (a) CV curves; (b) Discharge/charge profiles at a current density of 50 mA g^{-1}, and (c) Cycle performances of N-BCNTs at various current densities of 0.05, 0.1, 0.2, 0.5,1.0 and 0.1 A g^{-1}; (d) Cycle performances of N-BCNTs at the current density of 0.5 A g^{-1}. All experiments utilised a voltage range of 0.01-3.0 V *vs.* Na/Na$^+$.

The excellent sodium-ion storage performances of N-BCNTs might be attributed to its unique structure and composition. More specifically, the porous hollow structure exhibits a short Na$^+$ diffusion distance and a large electrode/electrolyte contact area, which are able to facilitate Na$^+$ diffusion and ultimately enhance rate capability.[7, 18, 20] Meanwhile, the hollow structure can provide ample space to accommodate volume changes that lead to excellent cycle stability.[8, 20, 32] Besides，their 1D structures could improve the electrical conductivity of N-BCNTs, which is in favour of enhancing the rate capability.[33] Furthermore, the doping nitrogen is able to further facilitate the diffusion of electric and Sodium-ion.[14-17, 19, 20] Inspired by their unique structure and composition, N-BCNTs were also tested as anode material for LIBs. The specific capacity measured as high as 574 mA h g^{-1} at a current density of 100 mA g^{-1}. Even at a high current density of 3 A g^{-1}, these N-BCNTs still possess a considerable capacity of 237 mA h g^{-1}. In addition, the N-BCNTs electrodes manifest outstanding cycle stability. Detailed results are shown in Fig. S9 (ESI†).

In summary, N-BCNTs were successfully prepared via a one-step pyrolysis process. When tested as anode materials for SIBs, the as-prepared N-BCNTs show high specific capacity, excellent cycle

stability and super rate capability due to their unique 1D porous hollow structure and high nitrogen doping. The specific capacity is as high as 270.6 mAh g^{-1} at a current density of 50 mA g^{-1}. Even at a current density of 1 A g^{-1}, N-BCNTs possess a capacity of 81 mAh g^{-1}. Considering their excellent cycle stability and the facile synthesis methodology, N-BCNTs should be considered for use as promising anode materials for SIBs.

Notes and references

1 N. Yabuuchi, K. Kubota, M. Dahbi and S. Komaba, *Chem. Rev.,* 2014, **114**, 11636.
2 H. Pan, Y. S. Hu and L. Chen, *Energy Environ. Sci.*, 2013, **6**, 2338.
3 S. W. Kim, D. H. Seo, X. Ma, G. Ceder and K. Kang, *Adv. Energy Mater.,* 2012, **2**, 710.
4 Z. Hu, L. Wang, K. Zhang, J. Wang, F. Cheng, Z. Tao and J. Chen, *Angew. Chem. Int. Ed.,* 2014, **126**, 13008.
5 S. Wenzel, T. Hara, J. Janek and P. Adelhelm, *Energy Environ. Sci.*, 2011, **4**, 3342.
6 T. Chen, L. Pan, T. Lu, C. Fu, D. H. Chua and Z. Sun, *J. Mater. Chem. A*, 2014, **2**, 1263.
7 K. Tang, L. Fu, R. J. White, L. Yu, M. M. Titirici, M. Antonietti and J. Maier, *Adv. Energy Mater.*, 2012, **2**, 873.
8 Y. S. Yun, S. Y. Cho, H. Kim, H. J. Jin and K. Kang, *ChemElectroChem*, 2015, **2**, 359.
9 T. Chen, Y. Liu, L. Pan, T. Lu, Y. Yao, Z. Sun, D. H. Chua and Q. Chen, *J. Mater. Chem. A*, 2014, **2**, 4117.
10 W. Luo, J. Schardt, C. Bommier, B. Wang, J. Razink, J. Simonsen and X. Ji, *J. Mater. Chem. A*, 2013, **1**, 10662.
11 J. Ding, H. Wang, Z. Li, A. Kohandehghan, K. Cui, Z. Xu, B. Zahiri, X. Tan, E. M. Lotfabad and B. C. Olsen, *ACS Nano*, 2013, **7**, 11004.
12 R. S. Babu and M. Pyo, *J. Electrochem. Soc.*, 2014, **161**, A1045.
13 E. M. Lotfabad, J. Ding, K. Cui, A. Kohandehghan, W. P. Kalisvaart, M. Hazelton and D. Mitlin, *ACS Nano*, 2014, **8**, 7115.
14 L. Fu, K. Tang, K. Song, P. A. van Aken, Y. Yu and J. Maier, *Nanoscale*, 2014, **6**, 1384.
15 H. G. Wang, Z. Wu, F. l. Meng, D. l. Ma, X. l. Huang, L. M. Wang and X. B. Zhang, *ChemSusChem*, 2013, **6**, 56.
16 Z. Wang, L. Qie, L. Yuan, W. Zhang, X. Hu and Y. Huang, *Carbon*, 2013, **55**, 328.
17 Z. S. Wu, W. Ren, L. Xu, F. Li and H. M. Cheng, *ACS Nano*, 2011, **5**, 5463.
18 Y. Cao, L. Xiao, M. L. Sushko, W. Wang, B. Schwenzer, J. Xiao, Z. Nie, L. V. Saraf, Z. Yang and J. Liu, *Nano lett.*, 2012, **12**, 3783.
19 J. Xu, M. Wang, N. P. Wickramaratne, M. Jaroniec, S. Dou and L. Dai, *Adv. Mater.*, 2015, **27**, 2042.
20 H. Song, N. Li, H. Cui and C. Wang, *Nano Energy*, 2014, **4**, 81.
21 J. Wang, H. Wu, D. Gao, S. Miao, G. Wang and X. Bao, *Nano Energy*, 2015, **13**, 387.
22 W. Yang, X. Liu, X. Yue, J. Jia and S. Guo, *J. Am. Chem. Soc.*, 2015, **137**, 1436.
23 D. Deng, L. Yu, X. Chen, G. Wang, L. Jin, X. Pan, J. Deng, G. Sun and X. Bao, *Angew. Chem. Int. Ed.,* 2013, **52**, 371.
24 Z. Wen, S. Ci, Y. Hou and J. Chen, *Angew. Chem. Int. Ed.,* 2014, **53**, 6496.

25 S. N. Mohammad, *Carbon*, 2014, **75**, 133.
26 C. J. Lee and J. Park, *Appl. Phys. Lett.*, 2000, **77**, 3397.
27 H. T. Chung, J. H. Won and P. Zelenay, *Nature Commun.*, 2013, **4**, 1922.
28 A. Primo, P. Atienzar, E. Sanchez, J. M. Delgado and H. García, *Chem. Commun.*, 2012, **48**, 9254.
29 C. Han, J. Wang, Y. Gong, X. Xu, H. Li and Y. Wang, *J. Mater. Chem. A*, 2014, **2**, 605.
30 D. Bhattacharjya, H. Y. Park, M. S. Kim, H. S. Choi, S. N. Inamdar and J. S. Yu, *Langmuir*, 2013, **30**, 318.
31 Z. Wang, X. Xiong, L. Qie, and Y. Huang, *Electrochim. Acta*, 2013, **106**, 320.
32 L. Zhang, G. Zhang, H. B. Wu, L. Yu and X. W. Lou, *Adv. Mater.*, 2013, **25**, 2589.
33 Q. Sun, X. Q. Zhang, F. Han, W. C. Li and A. H. Lu, *J. Mater. Chem.*, 2012, **22**, 17049.

ChemComm Accepted Manuscript